NUMERICAL SIMULATION OF ALTERNATING CURRENT LINEAR SWEEP VOLTAMMETRY AT MICRODISC ELECTRODES

David J. GAVAGHAN[+], Darrell M. ELTON[++] and Alan M. BOND[1,*]

School of Chemistry, Monash University, Clayton, Vic. 3800, Australia;
e-mail: [1] g.oliver@sci.monash.edu.au

Received November 16, 2000
Accepted December 8, 2000

Dedicated to the memory of the late Professor Antonín A. Vlček.

We extend our earlier work on the numerical simulation of ac linear sweep voltammetry at macroelectrodes to the case of microdisc electrodes. This requires the solution of the underlying diffusional transport equations in two dimensions, rather than one, using a cylindrical coordinate system. We use the two-dimensional FIRM algorithm combined with a specially designed exponentially expanding mesh. We examine the ac response as a function of the frequency and amplitude of the ac signal, and as a function of the non-dimensional parameter $p = (nFa^2v/RTD)^{1/2}$, where a is electrode radius, v the sweep rate, and D the diffusion coefficient. Results are analysed using Fast Fourier Transform (FFT) methods. We are able to derive a range of conditions under which radial diffusion has only a minor effect on the ac response of the system. The analytical results available for macroelectrodes therefore carry through to the microelectrode case for many practical ranges of system parameters (electrode size, dc sweep rate and diffusion coefficient). Experimental results are given which show good agreement with the numerical simulations.

Keywords: Alternating current voltammetry; Disc electrodes; FIRM algorithm; Fast Fourier Transform method; Electrochemistry.

Linear sweep and cyclic voltammetry, in their direct current (dc) modes, represent the most commonly employed techniques for elucidating mechanisms of electrode processes at both macro- and microdisc electrodes[1]. In principle, a more powerful approach to studying mechanisms of electrode processes is to use alternating current (ac) versions of dc linear sweep or cy-

+ Permanent address: Oxford University Computing Laboratory, Wolfson Building, Parks Rd., and Nuffield Dept. of Anaesthetics, University of Oxford, Radcliffe Infirmary, Oxford, U.K.
++ Permanent address: Department of Electronic Engineering, LaTrobe University, Bundoora, Vic. 3086, Australia

clic voltammetry[1–4]. In these techniques, an alternating potential (E_{ac} or ΔE) of known frequency (ω) is superimposed onto the waveform used in the dc techniques, and the ac response is then measured as a function of dc potential and frequency to extract the kinetics and thermodynamics. Consequently, a great deal of information additional to that available in dc voltammetry can be obtained. The advantage of ac linear sweep and ac cyclic voltammetry over their dc counterparts have been summarised by Bard and Faulkner[1].

However, unfortunately, theoretical solutions to the ac techniques are very limited compared to the dc case[1–4]. Furthermore, where solutions are available, suppositions commonly have been invoked which require that the dc and ac time scales are resolvable, and that the amplitude of the applied alternating potential is very small so that the theoretical solution may be linearised. In an earlier paper we therefore developed a numerical approach to the solution of ac voltammetry which allowed us to develop a more general theory which overcomes all of these restrictions[5] for the case of a macroelectrode.

In this paper we extend this earlier work to the case of the increasingly popular microdisc electrodes. This requires the solution of the underlying diffusional transport equations in two dimensions, rather than one, using a cylindrical coordinate system. The resulting equations are then solved using a two-dimensional FIRM algorithm (Fully implicit Richtmeyer modification) combined with a specially designed exponentially expanding mesh[6–8]. We examine the ac response for a microelectrode as a function of the frequency and amplitude of the ac signal. The effective size of the electrode can be controlled by varying a single non-dimensional parameter $p = (nFa^2v/RTD)^{1/2}$ (as defined by Aoki *et al.*[9]), where a is the electrode radius, v the sweep rate, and D the diffusion coefficient: small values of p correspond to a microdisc, and larger values of p tend to the macroelectrode case. All results are analysed in the frequency domain using Fast Fourier Transform (FFT) methods. We are able to derive a range of conditions under which radial diffusion has only a minor effect on the ac response of the system. The analytical results available for macroelectrodes therefore carry through to the microelectrode case for many practical ranges of system parameters (electrode size, dc sweep rate, and diffusion coefficient). Experimental results are given which show satisfactory agreement with the numerical simulations.

METHODS

Throughout this paper we will consider the case of a microdisc electrode. We will assume that semi-infinite mass transport occurs *via* diffusion only and we will make us of axial symmetry to assume that this process can be described in two-dimensional cylindrical coordinates. Assuming that the electrochemical oxidation reaction

$$\mathrm{A} \rightleftharpoons \mathrm{B} + n\,\mathrm{e} \tag{1}$$

takes place at the electrode surface, and mass transport can be described for each species s by

$$\frac{\partial c_s}{\partial t} = D_s \frac{\partial^2 c_s}{\partial r^2} + \frac{1}{r}\frac{\partial c_s}{\partial r} + \frac{\partial^2 c_s}{\partial z^2}\,, \tag{2}$$

where r and z are the radial and vertical spatial coordinates, respectively, t is time, c_s (r,z,t) is the concentration, and D_s the corresponding diffusion coefficient of each of the species s = A, B.

Boundary Conditions

Assuming that semi-infinite diffusion conditions are assumed, the following boundary and initial conditions result

$$\begin{aligned}
&z = 0,\quad r > a && \frac{\partial c_A}{\partial z} = 0 && \frac{\partial c_B}{\partial z} = 0\\
&z \geq 0,\quad r = 0 && \frac{\partial c_A}{\partial r} = 0 && \frac{\partial c_B}{\partial r} = 0\\
&z = 0,\quad r \leq a && D_A \frac{\partial c_A}{\partial z} = -D_B \frac{\partial c_B}{\partial z}\,, && D_A \frac{\partial c_A}{\partial z} = k_f c_A - k_b c_B\\
&z \to \infty,\ r \geq a && c_A = c_0 && c_B = 0\\
&z \geq 0,\quad r \to \infty && c_A = c_0 && c_B = 0\,,
\end{aligned} \tag{3}$$

where a is the electrode radius, k_f and k_b are the potential dependent rate constants for the forward and backward reactions and are given by

$$k_f = k_0 \exp\left(-\frac{\alpha nF}{RT}[E(t) - E^0]\right) = k_0 e^{-\alpha\tau}$$

$$k_b = k_0 \exp\left((1-\alpha)\frac{nF}{RT}[E(t) - E^0]\right) = k_0 e^{(1-\alpha)\tau}, \qquad (4)$$

where k_0 is the heterogeneous charge transfer rate constant at standard potential E^0, α is the charge transfer coefficient, $E(t)$ is the applied potential (see below), and τ is defined below in Eq. (*5*).

Throughout this paper, we will assume equal diffusion coefficients in all simulations, but it is of course obvious that cases involving unequal diffusion coefficients are equally tractable. In this special case ($D_A = D_B = D$ with c_B initially absent), it is straightforward to show that $c_B = c_0 - c_A$, and we need only solve for species A, with the corresponding simplification of the boundary conditions. We will also use a value of k_0 in Eq. (*4*) which is sufficiently high to ensure that reversible conditions apply, as detailed below, although computer codes are currently written to allow slow electron transfer.

Non-Dimensional Variables

We first introduce the following non-dimensional variables related to distance ($\tilde{r}$, $\tilde{z}$), time (τ), and concentration (u_A). To facilitate comparison with previous work[9,10], we introduce the following non-dimensional variables

$$\tilde{r} = r/a \quad \tilde{z} = z/a$$

$$u_A = c_A/c_0 \quad \tau = \frac{nF}{RT}\left(E_i + vt - E^0\right), \qquad (5)$$

where c_0 is the bulk concentration of species A, and E^0, n, F, R and T have their usual meanings. Substitution of each of these variables into Eq. (*2*) gives

$$\frac{1}{p^2}\left(\frac{\partial^2 u_A}{\partial \tilde{r}^2}+\frac{1}{\tilde{r}}\frac{\partial u_A}{\partial \tilde{r}}+\frac{\partial^2 u_A}{\partial \tilde{z}^2}\right)=\frac{\partial u_A}{\partial \tau}\,, \tag{6}$$

where

$$p=\left(\frac{nFa^2 v}{RTD}\right)^{1/2} \tag{7}$$

is the critical non-dimensional parameter determining the nature of the transport processes. As p gets large, diffusion tends to the linear process associated with macroelectrodes, and as p becomes small, diffusion tends towards the steady-state response at a microdisc (see, for example, Aoki *et al.*[9]).

The boundary conditions on $\tilde{r} = 0$, and $\tilde{z} = 0$ are identical for u_A, whilst the others become

$$\begin{aligned}
&\tilde{z} = 0, \quad \tilde{r} \le 1 \qquad \frac{\partial u_A}{\partial \tilde{z}} = \Lambda'\left[u_A\, e^{-\alpha\tau} - (1-u_A)\, e^{(1-\alpha)\tau}\right]\\
&\tilde{z} \to \infty, \quad \tilde{r} \ge 0 \qquad u_A = 1\\
&\tilde{z} \ge 0, \quad \tilde{r} \to \infty \qquad u_A = 1\,,
\end{aligned} \tag{8}$$

where

$$\Lambda' = k_0 a/D\,, \tag{9}$$

as introduced by Michael *et al.*[10], is a particularly suitable non-dimensional constant for numerical simulations, which we take to be equal to 10^6 throughout this paper to ensure fully reversible conditions.

Calculation of the Current

The current, $I(t)$, at the electrode surface is given by

$$I(t) = 2\pi nFD\int_0^a \left(\frac{\partial c_0}{\partial z}\right)_{z=0} r\,\mathrm{d}r\,. \tag{10}$$

In non-dimensional variables this becomes

$$I(\tau) = 2\pi nFDc_0 \int_0^1 \left(\frac{\partial u_A}{\partial \tilde{z}} \right)_{\tilde{z}=0} \tilde{r}\, d\tilde{r} . \qquad (11)$$

Throughout this paper we use the standard non-dimensionalisation for LSV (linear sweep voltammetry; see Chapter 6 of ref.[1]) giving a non-dimensional current density, and is the one used elsewhere[5]. It is given by

$$\tilde{I}(\tau) = I(\tau) \Big/ \left[nFAc_0 (\theta v D)^{1/2} \right], \qquad (12)$$

where $\theta = nF/RT$. This will allow us to compare our results to the corresponding results for macroelectrodes described in ref.[5].

Applied Potential for ac Voltammetry

The applied potential is defined in identical fashion to that described in ref.[5], where we showed that a particularly attractive representation for simulation of ac voltammetry arises by imposing the applied potential using the function

$$E(\tau) = \tau + \Delta\tau \sin(\Omega\tau), \qquad (13)$$

where Ω is the non-dimensional angular frequency, and $\Delta\tau$ is the amplitude of the oscilation. This allows us to define the rate of oscillation in the ac component in terms of the total number of oscillations, N, in a complete dc sweep. The duality in the interpretation of τ as either non-dimensional time or non-dimensional potential creates a slight problem in interpretation of results from non-dimensional variables in terms of dimensional variables. A detailed description of a method of translating from non-dimensional to dimensional variables and *vice versa*, making use of the fact that N must be the same in each case, can be found in ref.[5].

Numerical Methods

The two-dimensional diffusion equation and associated boundary conditions given above are solved numerically using a 6-level FIRM algorithm combined with an exponentially expanding mesh designed to give maximum error cancellation and near-optimal accuracy in the current for the

particular mesh size. This has been described previously[6–8], and was developed from the one-dimensional work of Rudolph and Feldberg and co-authors[11–14]. The reader is referred to these papers for fuller details. The simulated current is calculated from the concentration values using a three-point, second-order finite difference approximation (see, for example, ref.[15]).

Comparison with Analytical Results

Analytical results for linear diffusion at a macroelectrode have shown that provided the dc potential is held constant, at say E_{dc}, during the time that the ac signal is applied, then the system should have the following properties[16]:

– The peak of the ac wave at a particular angular frequency ω (which we will denote by I_p^{ac}), should be linear, within experimental error[17], in ΔE for amplitudes ≤ 8/n mV (assuming n = 1, this is equivalent to $\Delta\tau \leq 0.3$ in our non-dimensional variables).

– I_p^{ac} should be linear in $\omega^{1/2}$ (in the region in which it is linear, within experimental error[17], in ΔE).

– The phase shift between the applied potential and the fundamental harmonic ac wave should be 45°.

– If we consider the ac wave in terms of its harmonics, then the currents associated with the first (or fundamental) and second harmonics at small amplitudes[4,16] and other approximations referred to above, are given, in dimensional variables, by:

$$I(\omega) = \frac{n^2 F^2 A c_0 (\omega D)^{1/2} \Delta E}{4RT \cosh^2(j/2)} \sin\left(\omega t + \frac{\pi}{4}\right) \qquad (14)$$

$$I(2\omega) = \frac{2^{1/2} n^3 F^3 A c_0 (\omega D)^{1/2} (\Delta E)^2 \sinh(j/2)}{16 R^2 T^2 \cosh^3(j/2)} \sin\left(2\omega t - \frac{\pi}{4}\right), \qquad (15)$$

where $j = nF/RT(E_i - E^0)$. In non-dimensional variables this becomes[+++]

+++ Equations relating dimensional and non-dimensional variables are given in Eqs (*14*) to (*18*) of ref.[5].

$$I(\Omega) = \frac{\Delta\tau\sqrt{\Omega}}{4\cosh^2(\tau/2)} \sin\left(\Omega\tau + \frac{\pi}{4}\right) \quad (16)$$

$$I(2\Omega) = \frac{\Delta\tau^2\sqrt{\Omega}\sinh(\tau/2)}{16\cosh^3(\tau/2)} \sin\left(2\Omega\tau - \frac{\pi}{4}\right). \quad (17)$$

In addition, in our earlier work[5] we were able to show through numerical simulation that all of the above analytical results remain valid when the restriction that E_{dc} remains constant is lifted, provided that the dc and ac signals do not overlap in the frequency spectrum (we showed this to be a fairly weak constraint). The primary aim of this work is to ascertain whether similar relationships hold at microdisc electrodes, making use of the Fast Fourier Transform (FFT) method of analysis described in our earlier work[5].

EXPERIMENTAL

The chemical system used for the experimental investigations at microdisc electrodes was the oxidation of ferrocene in acetonitrile. All experiments were conducted using the following experimental parameters: a standard three-electrode cell with a 250 μm diameter gold working electrode, with platinum wire auxiliary and reference electrodes; 0.54 mM ferrocene, with 100 mM Bu_4NPF_6 supporting electrolyte, made up in acetonitrile (Mallinckrodt HPLC grade), and at a temperature of 19 °C. The potential was swept from 0 through to +550 mV at sweep rates of 39.74, 158.95, and 715.26 mV s^{-1}.

The voltammetric instrumentation was based on a conventional three-electrode potentiostat driven by a 19 bit delta sigma digital to analogue converter. The reference and working electrode potentials were digitised by separate 18 bit delta sigma analogue to digital converters. The system was run synchronously at a sample rate of 39.0625 kilosamples s^{-1}. All signal processing was performed using a portable computer with a 400 MHz Pentium II processor running Windows 98. All computer code was written in C++. The sampling rate was selected to ensure that each of the data sets in the experiments were 2^{15} bytes (32 768) in size so as to avoid aliasing and aid speed with the FFT processing. A moving average filter of 36, 9, and 2 was used for data collection at the above scan rates, respectively. The effective sampling rate was thus reduced to $1.085 \cdot 10^3$, $4.340 \cdot 10^3$, and $19.531 \cdot 10^3$ s^{-1}, respectively. The effect of this averaging was compensated for in the subsequent signal processing.

RESULTS

Testing the 2D Code

The numerical methods used have been described previously for accurate simulation of dc LSV at a microdisc[8]. This makes use of the FIRM algo-

rithm[11–14] combined with an exponentially expanding mesh designed to give maximal cancellation between the errors due to the boundary singularity (at the electrode edge) and the errors due to the numerical scheme throughout the solution region. We use the FIRM algorithm since we require a high degree of numerical stability for ac voltammetry where the boundary conditions change very rapidly with time. This will become crucial when considering methods such as square wave voltammetry which contains impulsive changes in the boundary conditions at each switch in potential (and may therefore cause oscillations with more computationally efficient numerical methods such as ADI (ref.[15])).

In this paper we are interested primarily in accuracy rather than in computational speed since we wish to demontrate the range of accuracy of the analytical results. We therefore use the very accurate "1%" mesh (see ref.[7]), which uses a very fine mesh in the vicinity of the electrode edge, and gives typical mesh sizes of around 100 × 40 (p = 10) up to 130 × 80 (p = 0.1) points. As usual, the numerical solution is obtained by replacing the semi-infinite region [0, ∞) × [0, ∞) by the finite region $[0, \tilde{r}_{max}] \times [0, \tilde{z}_{max}]$, and we follow Britz[17] in choosing $\tilde{r}_{max} = 1.0 + 6\sqrt{(\tau_{start} - \tau_{end})/p^2}$ and $\tilde{z}_{max} = 6\sqrt{(\tau_{start} - \tau_{end})/p^2}$ (since beyond this distance all concentration values will effectively equal the bulk concentration).

The level of accuracy of the numerical method is compared with the analytic solution of Aoki *et al.*[9] in Fig. 1 of ref.[8]. There it was shown that the maximum difference between the analytic and numerical solutions for the dc current was less than 0.25% for all values of p between 0.1 and 10.0.

For ease of reference, the way in which the non-dimensional parameter $p = (nFa^2v/RTD)^{1/2}$ varies with dimensional values of electrode radius a and sweep rate v is shown in Table I assuming n = 1, $D = 1.0 \cdot 10^{-9}$ m^2 s^{-1}, and T = 25 °C. It can be seen that values of $p < 1$ correspond either to a very small electrode radius or to a very slow sweep rate.

FFT Analysis of the dc Component

All analyses of results will again be performed in the frequency domain using the FFT method as in our analysis of the one-dimensional planar diffusion case[5]. Clearly in the 1D case, we have only one background dc signal (the dashed line in Fig. 1a) and determining when the ac and dc components are separate in the frequency domain is straightforward. However, for a microdisc, the background dc signal is a function of the parameter p (the full lines in Fig. 1a), and its frequency spectrum becomes increasingly broad

as p decreases, as shown in Fig. 1b. As a result, for smaller values of p, we will be forced to use increasingly large values of the frequency for the ac component to ensure that overlap between the dc and ac spectra is sufficiently small to allow recovery of the ac signal without excessive interference from the dc signal.

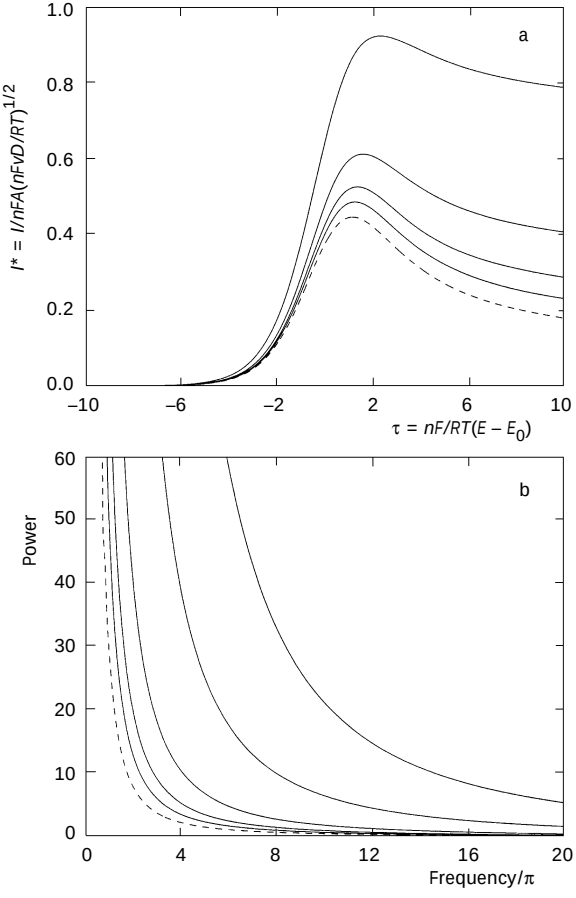

FIG. 1
The effect of increasing p on the dc signal. The highest curve corresponds to $p = 2$, then $p = 5$, 10, 20, and 50 (full lines) with the dashed line giving the response for a macroelectrode corresponding to $p = \infty$. (a) Represents the dc voltammetric response and (b) the power spectra of the dc signals

Numerical Simulation of ac Voltammetry

Figure 2a shows the numerical simulations for ac voltammetry at a microdisc for values of p = 1, 2, and 10, corresponding to either an increasing electrode radius or an increasing sweep rate, for $\Omega = 8\pi$ and $\Delta\tau = 0.1$. The most striking feature of these figures is that the amplitude of the ac oscillation does not appear to vary very much as p decreases. The corresponding power spectra are shown in Fig. 2b.

If we filter out the dc signal using the FFT method described in ref.[5], we obtain the results shown in Fig. 3. For the two cases shown, p = 1 and 10, we see that the main difference is in the amount of noise indtroduced at the edges of the spectrum by the interference from the dc signal. The ac response remains very similar, with peak current values of 0.1410 for p = 1, 0.1326 for p = 2, and 0.1265 for p = 10, compared to the changes in the dc peak currents which are 1.510, 0.9231, and 0.5257, respectively. The analytical peak ac current derived using one-dimensional theory is 0.1253, and that for the dc sweep is 0.4463. So whilst the peak current of the ac wave changes by only 12.5, 5.8, and 1.0% for p = 1, 2, and 10, respectively, compared to the planar case, the corresponding changes in the peak of the dc wave are 238, 107, and 18%. This suggests that under certain (derivable) conditions, the analytic solution of Eq. (*14*), which we showed in our earlier paper to be valid at all times for the one-dimensional macroelectrode

TABLE I
The variation in $p = (nFa^2v/RTD)^{1/2}$ with the dimensional variables of electrode radius a (in μm) and sweep rate v assuming that n = 1, $D = 1.0 \cdot 10^{-9}$ m^2 s^{-1}, and T = 25 °C

v, V s^{-1}	p			
	a = 5	a = 10	a = 20	a = 50
100.0	9.86	19.7	39.5	98.6
10.0	3.12	6.24	12.5	31.2
1.0	0.986	1.97	3.95	9.86
0.1	0.312	0.624	1.25	3.12
0.01	0.0986	0.197	0.395	0.986
0.001	0.0312	0.0624	0.125	0.312

case, will also be valid to within a small error for the microdisc case. Below we give an analysis of the dependence of the ac signal at a microdisc on the frequency and on the parameter p, and use this to derive simple conditions on p and ω, the dimensional angular frequency, for which the analytical Eq. (*14*) for the macroelectrode case can be used for the microdisc to within 1%. All of the other properties of the analytical solution (linearity of peak current with $\Delta\tau$ and $\Omega^{1/2}$, and a phase shift of $\pi/4$) are then shown to follow automatically to a similar degree of accuracy.

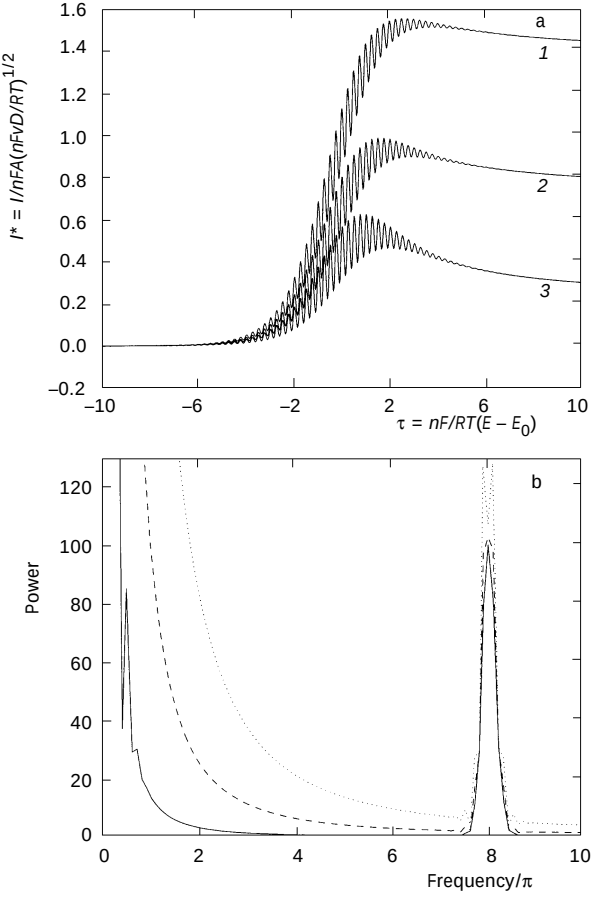

FIG. 2

The combined ac and dc signals for p = 1 (*1*), 2 (*2*), and 10 (*3*) with $\Omega = 8\pi$ and $\Delta\tau = 0.1$ (a), and the power spectra of each of these signals (dotted line is p = 1, dashed line is p = 2, full line is p = 10) (b)

Dependence of the ac Signal on p and Ω

The dependence of the peak current of the ac wave is given in Table II as a function of both the frequency, Ω, and the non-dimensional parameter $p = (nFa^2v/RTD)^{1/2}$, and in brackets we give the associated phase angles. Also shown in the final column of Table II is the dependence of the dc peak on p. In Table III we give the absolute change and the percentage change in the ac peak current with both p and Ω, and the percentage change in the dc

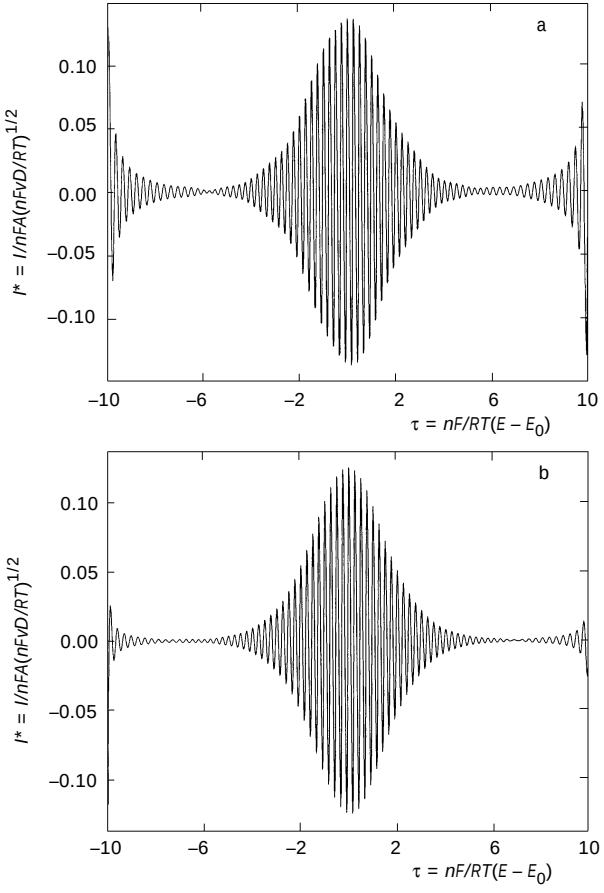

FIG. 3
The ac signals recovered using FFT filtering for $p = 1$ (a) and $p = 10$ (b); $\omega = 8\pi$ and $\Delta\tau = 0.1$ in both cases

peak as a function of p, calculated from the values given in Table II. As suggested above, the effects of radial diffusion on the ac component of the signal are very much smaller for a given value of p than on the dc component, and the effects also decrease with increasing frequency. Reading across the columns of Table III for particular values of p, it is clear that the absolute change due to radial diffusion effects remain fixed, *i.e.*, is independent of Ω (to within numerical error) as Ω is varied. The phase angles give the expected 45° at high p values and high frequencies, but give smaller values at lower values of p due to interaction between the ac and dc spectra in the frequency domain.

These effects can be explained in terms of the differences between the time scales of the ac and dc components of the current. The typical timescale of the dc sweep, say t_{dc}, is the range of τ values over which the current is changing in a time-dependent manner, and from Figs 1 and 2 it can be seen that a value of the order of 10 (in non-dimensional variables) is a reasonable choice covering all values of p. The typical diffusion layer thickness is then given by $\delta_{dc} = \sqrt{2Dt_{dc}} = \sqrt{2t_{dc} / p^2}$ (see p. 129 of ref.[1]). That is, the diffusion layer thickness is proportional to $1/p$.

TABLE II

The variation in the peak current of the ac wave as a function of the frequency, Ω, and the non-dimensional parameter $p = (nFa^2\nu/RTD)^{1/2}$ (columns 1 to 5), and in parentheses the associated phase angle in degrees, and the variation of the dc peak current with p (column 6). In all cases the amplitude of the ac signal is $\Delta\tau = 0.1$

p	Peak current of ac wave					dc Peak
	$\Omega = 4\pi$	$\Omega = 8\pi$	$\Omega = 16\pi$	$\Omega = 32\pi$	$\Omega = 64\pi$	
∞	0.0886 (45.0)	0.1253 (45.0)	0.1772 (45.0)	0.2507 (45.0)	0.3544 (45.0)	0.4463
50	0.0890 (44.8)	0.1259 (44.9)	0.1777 (44.9)	0.2512 (44.9)	0.3552 (44.9)	0.4611
20	0.0895 (44.5)	0.1264 (44.6)	0.1782 (44.8)	0.2516 (44.8)	0.3555 (44.9)	0.4841
10	0.0904 (43.9)	0.1272 (44.2)	0.1789 (44.5)	0.2524 (44.6)	0.3563 (44.7)	0.5257
5	0.0921 (42.8)	0.1290 (43.4)	0.1807 (44.0)	0.2541 (44.3)	0.3580 (44.5)	0.6145
2	0.0976 (39.7)	0.1346 (41.1)	0.1859 (42.4)	0.2593 (43.1)	0.3631 (43.6)	0.9231
1	0.1077 (34.9)	0.1444 (37.5)	0.1950 (39.8)	0.2682 (41.2)	0.3720 (42.3)	0.1511
0.5	0.1309 (37.0)	0.1663 (31.1)	0.2147 (35.0)	0.2871 (37.7)	0.3905 (39.1)	2.750

Analogously, the typical time scale of ac signal is proportional to the period of the oscillation, or more precisely, $t_{ac} = T_\Omega/4$, or one quarter of the period of the oscillation, since in this time interval the ac component moves from the underlying dc potential to its peak value, before returning back to the underlying dc potential. The typical diffusion layer thickness of the ac component is therefore $\delta_{ac} = \sqrt{2Dt_{ac}} = \sqrt{2t_{ac} / p^2} = \sqrt{\pi\Omega / p^2}$, since $T_\Omega = 2\pi/\Omega$. The diffusion layer thickness for the ac component is therefore proportional to $1/p\Omega^{1/2}$, and will be considerably smaller than that for the dc component as Ω increases. Since the diffusion layer thickness gives a rule-of-thumb estimate of how far out into the bulk solution (from the electrode surface) transport processes are active both radially and vertically from the electrode surface, we can expect that radial diffusion will have a markedly lessened effect on the ac component compared to the dc component, as we have seen in Table II.

TABLE III

The absolute and the percentage change (in parentheses) in the peak current of the ac wave as a function of the frequency, Ω, and the non-dimensional parameter $p = (nFa^2v/RTD)^{1/2}$ (columns 1 to 5). The percentage change in the dc peak current with p (column 6)

p	Absolute and percentage change (%) in ac peak with p, Ω					% change dc peak
	$\Omega = 4\pi$	$\Omega = 8\pi$	$\Omega = 16\pi$	$\Omega = 32\pi$	$\Omega = 64\pi$	
50	$3.8 \cdot 10^{-4}$ (0.4%)	$5.7 \cdot 10^{-4}$ (0.5%)	$5.0 \cdot 10^{-4}$ (0.3%)	$5.7 \cdot 10^{-4}$ (0.2%)	$7.3 \cdot 10^{-4}$ (0.2%)	3.3
20	$8.6 \cdot 10^{-4}$ (1.0%)	$1.1 \cdot 10^{-3}$ (0.8%)	$9.4 \cdot 10^{-4}$ (0.5%)	$9.7 \cdot 10^{-4}$ (0.3%)	$1.05 \cdot 10^{-4}$ (0.3%)	8.7
10	$1.7 \cdot 10^{-3}$ (1.9%)	$1.9 \cdot 10^{-3}$ (1.5%)	$1.8 \cdot 10^{-3}$ (1.0%)	$1.8 \cdot 10^{-3}$ (0.7%)	$1.8 \cdot 10^{-3}$ (0.5%)	17.8
5	$3.5 \cdot 10^{-3}$ (3.9%)	$3.7 \cdot 10^{-3}$ (2.9%)	$3.4 \cdot 10^{-3}$ (1.9%)	$3.4 \cdot 10^{-3}$ (1.4%)	$3.5 \cdot 10^{-3}$ (1.0%)	37.7
2	$9.0 \cdot 10^{-3}$ (10.1%)	$9.2 \cdot 10^{-3}$ (7.3%)	$8.7 \cdot 10^{-3}$ (4.9%)	$8.6 \cdot 10^{-3}$ (3.4%)	$8.6 \cdot 10^{-3}$ (2.4%)	107
1	$1.9 \cdot 10^{-2}$ (21.4%)	$1.9 \cdot 10^{-2}$ (15.2%)	$1.8 \cdot 10^{-2}$ (10.0%)	$1.8 \cdot 10^{-2}$ (7.0%)	$1.8 \cdot 10^{-2}$ (4.9%)	239
0.5	$4.2 \cdot 10^{-2}$ (47.7%)	$4.1 \cdot 10^{-2}$ (32.6%)	$3.8 \cdot 10^{-2}$ (21.1%)	$3.7 \cdot 10^{-2}$ (14.6%)	$3.6 \cdot 10^{-2}$ (10.2%)	516

This allows us to give a rough estimate of the extent to which radial diffusion might affect the ac signal. For example, a value of $p = 150$ corresponds to a $\delta_{dc} = 0.03$ and the corresponding dc peak current is 0.4512, *i.e.*, an increase of about 1%. We would therefore expect errors of around 1% in the ac peak current whenever the value of $\delta_{ac} \approx 0.03$, which is the case, for example, for $p = 5$ and $\omega = 32\pi$ ($\delta_{dc} = 0.035$), and for $p = 10$, $\omega = 8\pi$ ($\delta_{dc} = 0.035$) and in these cases the ac peak flux is increased by 1.3 and 0.97%, respectively. From this heuristic analysis, we conclude that the peak of the ac wave for a microelectrode takes the approximate form

$$I_p^{ac} = \Omega^{1/2} \Delta\tau \left(a + \frac{b}{\Omega^{1/2} p} \right) \tag{18}$$

$$= \Delta\tau \left(a\Omega^{1/2} + \frac{b}{p} \right), \tag{19}$$

where a and b are constants, and we expect that $a = 1/4$ in non-dimensional variables from the 1D analysis (see Eq. (*21*) of ref.[5]). Both a and b can be approximated by multiple linear regression of I_p^{ac} against $\Delta\tau\Omega^{1/2}$ against $\Delta\tau/p$ calculated using the values given in Table II. This gives a value of $b = 0.1707$ and a value of $a = 0.250$ (as expected), and a regression R^2 coefficient of 0.999996, so that agreement is well within the numerical error of the simulation.

Comparison of 1D Analytic and 2D Numerical Simulation Results

The implications of the above are that provided that p and/or Ω are sufficiently large, the distortion of the ac signal due to radial diffusion is quantifiably small. A respectable level of experimental accuracy is 5%, whilst errors of 2% are considered excellent. So, provided that the level of distortion due to radial diffusion is less than, say, 1%, it will not be observable experimentally. Using Eq. (*19*) we require that

$$\frac{b}{p} < 0.01 a \Omega^{1/2} \tag{20}$$

or, equivalently,

$$\Omega^{1/2} p > \frac{b}{0.01a} \approx 70. \tag{21}$$

Since in dimensional coordinates the angular frequency $\omega = \theta v \Omega$, this is equivalent to a requirement that

$$\frac{a\omega^{1/2}}{D} = 70. \qquad (22)$$

So, for example, if the diffusion coefficient were $1 \cdot 10^{-9}$ m^2 s^{-1} and a = 250 μm, then the radial component of the ac signal would be less than 1% provided that $\omega > 78$ rad s^{-1} or 12.5 Hz.

Provided that these conditions are met, we can dispense with the numerical solution and simply use the analytic solution of Eq. (*14*). This is illustrated in Fig. 4, where we have superimposed the analytic solution for $\Omega = 4\pi$, p = 10, and $\Delta\tau$ = 0.1 on top of the numerical simulation at the same parameter values. As can be seen, other than a slight increase in the simulated current at each turning point (up to a maximum of about 0.96%, see Table II), the two lie on top of one another. Under these conditions, all of the results quoted earlier for macroelectrodes derived using one-dimensional theory will remain valid for the two-dimensional microdisc.

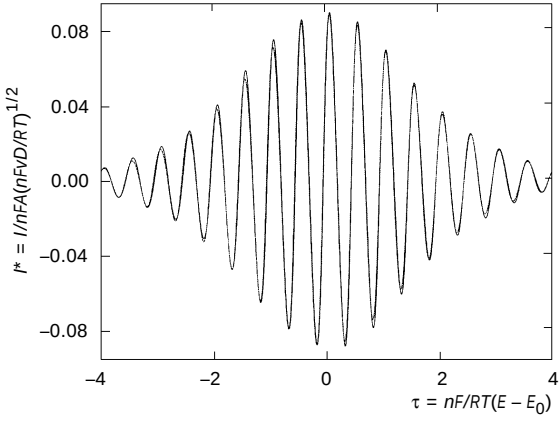

FIG. 4

The analytic solution of Eq. (*14*) which assumes 1D linear diffusion is plotted on top of the simulated solution for 2D cylindrical diffusion for p = 10, $\Omega = 4\pi$, and $\Delta\tau$ = 0.1. The peak current for the 2D simulation is increased by about 0.96% due to the effects of radial diffusion (see Table II)

Experimental Results

Experimental confirmation of our theoretical results is given in Figs 5 and 6, where the chemical system under investigation is the one-electron oxidation of ferrocene in acetonitrile. This process is close to reversible, but exhibits a small level of non-ideality at macrodisc electrodes in acetonitrile[18–20]. A variation in p was achieved by varying the scan rate while maintaining a fixed electrode radius.

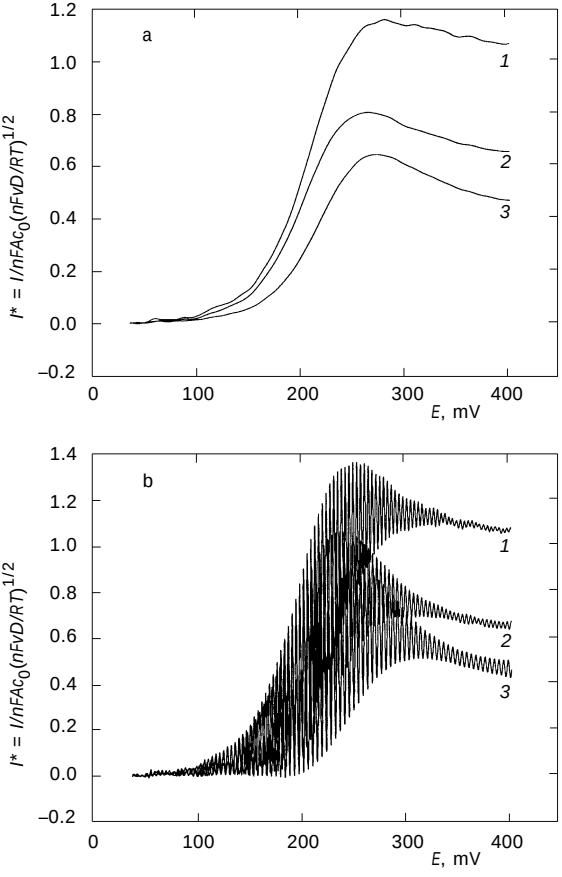

FIG. 5
The dc signal (a) and the combined ac and dc signals (b) for p = 1.6 (*1*), 3.2 (*2*), and 10 (*3*). Conditions: 0.54 mM ferrocene in MeCN, 125 μm gold electrode, amplitude 5 mV

The dc current shown in Fig. 5a was separated from the combined signal as shown in Fig. 5b using FFT processing. These currents were then made non-dimensional by

$$I^*(t) = I(t) \Big/ \left[nFAc_0 \left(nFvD/RT \right)^{1/2} \right]. \qquad (23)$$

This allows us to directly compare our results to the corresponding simulation results for macrodisc electrodes shown in Figs 1a and 2a. The experi-

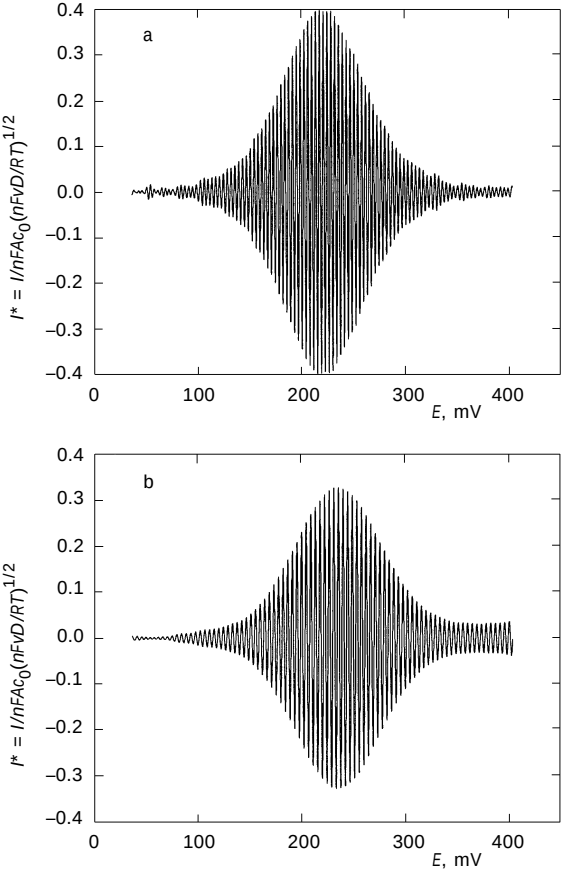

FIG. 6
The ac signals recovered using FFT filtering for p = 1.6 (a) and 6.8 (b). Conditions as in Fig. 5

mental dc current was within 10% of the simulation value for all three values of p. An applied ac amplitude of 5 mV was used which corresponds to $\Delta\tau = 0.2$ thus the ac perturbations shown in Fig. 5b are larger than that shown in the corresponding simulation results in Fig. 2a.

Figures 6a and 6b were obtained using FFT processing on the combined signals of Fig. 5b for $p = 1.6$ and 6.8, respectively. The non-zero ac amplitude for potentials beyond 400 mV was believed to be due to adsorption at the gold electrode, which is more apparent at higher scan rates (larger p). The peak ac amplitude of the both waves shown in Fig. 6 are the same within 5% after a normalising correction is applied to the perturbation frequencies. The corresponding phase angles were within 3° of the expected 45° for all experimental values of p.

Computing

All codes are written in Fortran and were run on an IBM ThinkPad portable PC with a 366 MHz processor. The FFTs, graphics, and statistical analyses were performed using Matlab[21]. All codes are available from the authors upon request.

Conclusions

Good qualitative agreement between theoretical and experimental results was achieved and confirms the suitability of using an analysis in the frequency domain for ac voltammetry at microdisc electrodes. Work is presently in progress to establish the quantitative accuracy of this analysis for a wider range of chemical systems.

REFERENCES

1. Bard A. J., Faulkner L. R.: *Electrochemical Methods*. John Wiley and Sons, New York 1980.
2. Rieger P. H.: *Electrochemistry*, 2nd ed., p. 366. Chapman and Hall, New York–London 1994.
3. Brett M. A., Brett A. M. O.: *Electrochemistry: Principles, Methods and Applications*, p. 238. Oxford University Press, Oxford 1993.
4. Bond A. M.: *Modern Polarographic Methods in Analytical Chemistry*, p. 341. Marcel Dekker, New York 1980.
5. Gavaghan D. J., Bond A. M.: *J. Electroanal. Chem.* **2000**, *480*, 133.
6. Gavaghan D. J.: *J. Electroanal. Chem.* **1998**, *446*, 1.
7. Gavaghan D. J.: *J. Electroanal. Chem.* **1998**, *446*, 13.
8. Gavaghan D. J.: *J. Electroanal. Chem.* **1998**, *446*, 25.
9. Aoki K., Akimoto K., Tokuda K., Matsuda H.: *J. Electroanal. Chem.* **1984**, *171*, 219.

10. Michael A. C., Wightman R. M., Amatore C. A.: *J. Electroanal. Chem.* **1989**, *267*, 33.
11. Rudolph M.: *J. Electroanal. Chem.* **1991**, *314*, 13.
12. Rudolph M.: *J. Electroanal. Chem.* **1995**, *338*, 85.
13. Mocak J., Feldberg S. W.: *J. Electroanal. Chem.* **1994**, *378*, 31.
14. Feldberg S. W., Goldstein C. I.: *J. Electroanal. Chem.* **1995**, *397*, 1.
15. Gavaghan D. J.: *J. Electroanal. Chem.* **1997**, *420*, 147.
16. Smith D. E. in: *Electroanalytical Chemistry* (A. J. Bard, Ed.), p. 1. Marcel Dekker Inc., New York 1966.
17. Britz D.: *Digital Simulation in Electrochemistry*, 2nd ed. Springer, Heidelberg 1988.
18. Rivera I. M., Cabera C. R.: *J. Electrochem. Soc.* **1993**, *140*, 636.
19. Dashback J., Blackwood D., Pons D., Pons S.: *J. Electroanal. Chem.* **1987**, *140*, 636.
20. Bond A. M., Snook G. A., Oldham K. B.: *Anal. Chem.* **2000**, *72*, 3492.
21. *Using Matlab 5.2*. The MathWorks Inc., Natick (MA) 1998.